Available online at www.sciencedirect.com

ScienceDirect

Procedia Structural Integrity 8 (2018) 433–443

Structural Integrity Procedia

www.elsevier.com/locate/procedia

AIAS 2017 International Conference on Stress Analysis, AIAS 2017, 6-9 September 2017, Pisa, Italy

Radial basis functions mesh morphing for the analysis of cracks propagation

M.E. Biancolini[a], A. Chiappa[a], F. Giorgetti[a], S. Porziani[a]*, M. Rochette[b]

[a]*University of Rome "Tor Vergata", Rome 00133, Italy*
[b]*ANSYS France, 11 Avenue Albert Einstein, 69100 Villeurbanne, France*

Abstract

Damage tolerant design requires the implementation of effective tools for fracture mechanics analysis suitable for complex shaped components. FEM methods are very well consolidated in this field and reliable procedures for the strength assessment of cracked parts are daily used in many industrial fields. Nevertheless the generation of the computational grid of the cracked part and its update after a certain evolution are still a challenging part of the computational workflow. Mesh morphing, that consists in the repositioning of nodal locations without changing the topology of the mesh, can be a meaningful answer to this problem as it allows the mesh updating without the need of rebuilding it from scratch. Fast Radial Basis Functions (RBF) can be used as an effective tool for enabling mesh morphing on very large meshes that are typically used in advanced industrial applications (many millions of nodes). The applicability of this concept is demonstrated in this paper exploiting state of the art tools for FEA (ANSYS Mechanical) and for advanced mesh morphing (RBF Morph ACT Extension). Proposed method is benchmarked using as a reference a circular notched bar with a surface defect. Reliability of fracture parameter extraction on the morphed mesh is first verified using as a reference literature data and ANSYS Mechanical tools based on re-meshing: different crack shapes are achieved using the new geometry as a morphing target. Crack propagation workflow is then demonstrated showing the computed shape evolution for different size and shape of the initial crack.

Peer-review under responsibility of the Scientific Committee of AIAS 2017 International Conference on Stress Analysis

Keywords: RBF; Fracture Analysis; Notched Bars; Crack Growth; Mesh Morphing

* Corresponding author. Tel.: *+39 06 72597136*.
E-mail address: porziani@ing.uniroma2.it

Peer-review under responsibility of the Scientific Committee of AIAS 2017 International Conference on Stress Analysis
10.1016/j.prostr.2017.12.043

1. Introduction

It is well known that the fatigue life of a structural component copes with the initiation and propagation of a crack. Under cyclic loading, a flaw may appear on the surface of the material and progressively grow until its size becomes critical. On the other hand, singularities introduced in the shape of a structure are preferential sites of crack initiation. This is due to the local stress increase that they provoke and, possibly, to the surface damage that machining could have caused. It is thus reasonably that these two circumstances are supposed to work together. Several authors (Carpinteri et al. (2003), Lin and Smith (1998), Murakami (1986), Guo et al. (2003), Biancolini and Brutti (2002)) dealt with the issue of a notched round bar with a crack in the reduced cross-section. The Stress-Intensity Factors (SIFs) are deduced through a Finite Element (FE) approach, which can keep into account the influence of the notch on the crack. The fatigue propagation paths of the fracture can be determined by employing the Paris-Erdogan law (Paris and Erdogan (1963)). The shape of the crack front changes after each cyclic loading step, according to the current values of the SIFs. The study of the subsequent configurations that the crack assumes during its evolution is a challenging task (Galland et al. (2011)). Each advancement of the front entails an updating of the mesh, which can result annoying and rather time-consuming if led by hand. This last consideration suggests the idea that is at the basis of the present paper. Mesh morphing techniques (Staten et al. (2011), de Boer et Al. (2007), Biancolini (2011)) allow a fast arrangement of the existing mesh to a new configuration. This enables an implementation of design variations, which is much faster than re-meshing the entire body from scratch. A large number of different crack front geometries can be derived morphing a baseline configuration. Time spent to obtain the FE model would reduce drastically, and furthermore, the simulation of crack growth could be automatized through an analysis-and-update procedure. Many methods are actually available to put in practice the just described process. A rough distinction can be made upon the role played by the mesh: mesh morphing methods can be categorized as either mesh-based or mesh-less. Our choice fell on a meshless approach, in particular the one implemented by the tool RBFMorph^{TM}. Radial Basis Functions (RBF) constitute its mathematical background. They are real-valued functions, taken from the Approximation Theory. Some basic concepts about RBF are given in the next section. Mesh morphing based on RBF proved to give excellent results in many practical examples (Biancolini and Cella (2010), Biancolini and Groth (2014), Cella et al. (2017)). Its major drawback is that, despite its meshless working principle, element topology does not change during the morph operation. This last foresees a simple displacement of node locations and the extent of morph must take into account degeneration of mesh quality.

The activities presented in this work were financially supported by the RBF4CRACKS project funded by the University of Rome "Tor Vergata" under the program "Consolidate the Foundations".

Nomenclature

a	Crack depth
b	Semi span of the crack
CD	Circumferential Divisions: number of angular divisions of crack tube
D	Bar diameter in the un-notched cross section
D_0	Bar diameter in the notched cross section
F	Applied force to the bar
FE	Finite Element
FT	Fracture Tool
L	Bar length, $L = 4D$
LCR	Largest Contour Radius of wedge elements around the crack front
N_{cyc}	Number of cycles related to crack growth
RD	Radial Division of crack tube
RBF	Radial Basis Functions
α	Crack aspect ratio, $\alpha = a/b$
σ_F	Nominal tensile stress referred to the reduced cross-section
ζ	Curvilinear abscissa along the crack front

ζ^*	Dimensionless curvilinear abscissa $\zeta^* = \zeta/h$

1.1. Background on RBF

RBF were introduced in the early 60s to manage problems of multidimensional interpolation (Davis (1963)). If data are given in the form of scattered scalar values at a series of point $\boldsymbol{x}_{\boldsymbol{k}_i}$ in the space $\mathbb{R}^n$, an interpolator s is introduced in order to have an approximating smooth function in the same space. At a location $\boldsymbol{x}$ its value is

$$s(\boldsymbol{x}) = \sum_{i=1}^{N} \gamma_i \varphi\left(\left\|\boldsymbol{x} - \boldsymbol{x}_{\boldsymbol{k}_i}\right\|\right) \tag{1}$$

The above summation is extended to all the points N where data are given, called source points. The point at which the value is retrieved is a target point. φ is the so-called radial basis function, namely a defined scalar function of the Euclidean distance between source and target points. γ_i are weights of the radial basis, for their computation a linear system of equations, whose order is equal to the number of source points introduced, needs to be solved. Typical RBF are shown in Table 1, if $r = \left\|\boldsymbol{x} - \boldsymbol{x}_{\boldsymbol{k}_i}\right\|$.

Table 1. Most common Radial Basis Functions

RBF	Column A (t)
Spline type (Rn)	$r^n, n\ odd$
Thin plate spline	$r^n \log(r), n\ even$
Multiquadric (MQ)	$\sqrt{1+r^2}$
Inverse multiquadric (IMQ)	$\frac{1}{\sqrt{1+r^2}}$
Inverse quadric (IQ)	$\frac{1}{1+r^2}$
Gaussian (GS)	e^{-r^2}

Sometimes, the radial basis interpolator has to be slightly modified in order to guarantee the existence and the uniqueness of the solution. This is obtained with a polynomial part h that is added to the form presented in (1).

$$s(\boldsymbol{x}) = \sum_{i=1}^{N} \gamma_i \varphi\left(\left\|\boldsymbol{x} - \boldsymbol{x}_{\boldsymbol{k}_i}\right\|\right) + h(\boldsymbol{x}) \tag{2}$$

The degree of the polynomial depends on the kind of RBF adopted.

If g_i are the given values at the source points $\boldsymbol{x}_{\boldsymbol{k}_i}$, a radial basis fit exists if the coefficients γ_i and the weights of the polynomial can be found such that the following conditions are satisfied:

$$\begin{aligned} &s(\boldsymbol{x}_{\boldsymbol{k}_i}) = g_i \\ &h(\boldsymbol{x}_{\boldsymbol{k}_i}) = 0 \end{aligned} \qquad 1 \le i \le N \tag{3}$$

A condition of orthogonality is also required

$$\sum_{i=1}^{N} \gamma_i p\left(\boldsymbol{x}_{\boldsymbol{k}_i}\right) = 0 \tag{4}$$

for all polynomials p with a degree less or equal than that of polynomial h. A unique interpolator exists if the basis function is a conditionally positive definite function. If a linear polynomial is chosen in a 3D space

$$h(\boldsymbol{x}) = \beta_1 + \beta_2 x + \beta_3 y + \beta_4 z \tag{5}$$

a non-singular square system can be obtained as follows

$$\begin{bmatrix} \mathbf{M} & \mathbf{P} \\ \mathbf{P}^{\mathrm{T}} & 0 \end{bmatrix} \begin{pmatrix} \boldsymbol{\gamma} \\ \boldsymbol{\beta} \end{pmatrix} = \begin{pmatrix} \boldsymbol{g} \\ 0 \end{pmatrix} \tag{6}$$

M is the interpolation matrix

$$M_{ij} = \varphi\left(\boldsymbol{x}_{\boldsymbol{k}_i} - \boldsymbol{x}_{\boldsymbol{k}_j} \right) \qquad 1 \le i, j \le N \tag{7}$$

P is a constraint matrix due to the orthogonality condition

$$\mathbf{P} = \begin{bmatrix} 1 & x_{k_1} & y_{k_1} & z_{k_1} \\ 1 & x_{k_2} & y_{k_2} & z_{k_2} \\ \vdots & \vdots & \vdots & \vdots \\ 1 & x_{k_N} & y_{k_N} & z_{k_N} \end{bmatrix} \tag{8}$$

In mesh-morphing applications, it is evident that RBF have to handle a vector field of displacement. In these cases, each component is interpolated as an independent scalar field:

$$\begin{cases} s_x(\boldsymbol{x}) = \sum_{i=1}^{N} \gamma_i^x \varphi\left(\boldsymbol{x} - \boldsymbol{x}_{\boldsymbol{k}_i} \right) + \beta_1^x + \beta_2^x x + \beta_3^x y + \beta_4^x z \\ s_y(\boldsymbol{x}) = \sum_{i=1}^{N} \gamma_i^y \varphi\left(\boldsymbol{x} - \boldsymbol{x}_{\boldsymbol{k}_i} \right) + \beta_1^y + \beta_2^y x + \beta_3^y y + \beta_4^y z \\ s_z(\boldsymbol{x}) = \sum_{i=1}^{N} \gamma_i^z \varphi\left(\boldsymbol{x} - \boldsymbol{x}_{\boldsymbol{k}_i} \right) + \beta_1^z + \beta_2^z x + \beta_3^z y + \beta_4^z z \end{cases} \tag{9}$$

Nodes that have to move are the selected source points with an assigned displacement. The morphing action is restricted to the desired zones of the mesh simply prescribing a null motion to those nodes that wrap the affected area. It is well said that the outcome of the morphing operation and the preservation of mesh quality depend on the skill of the user that performs the task. Anyway, in the remainder of the paper, details are given to properly steer the morphing action to success.

2. Application description

The proposed workflow is built completely in ANSYS® Workbench™. A round bar presents a circumferential notch with a constant curvature radius ρ, as depicted in Fig. 1b. The diameter of the bar is equal to D in an un-notched cross-section and D_0 in the reduced cross-section. The circular section of the groove has its center on the cylindrical

surface of the bar, so that $D_0 = D - 2\rho$. Total lenght of the bar is $4D$, supposed enough to extinguish any boundary effect well before the flawed region. The bar is fixed at one edge and loaded by an axial force at the opposite.

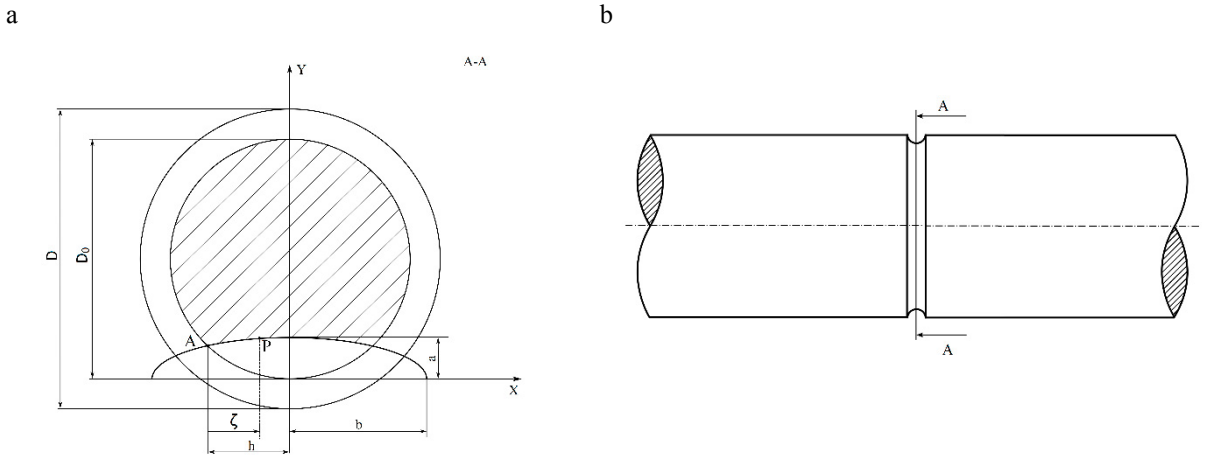

Fig. 1. (a) Semi-elliptical crack front geometry; (b) Notched bar geometry.

The parameter set necessary to build and load the model is shown in Table 2. Crack modelling is embedded in ANSYS® Mechanical by means of the Fracture Tool (FT). This tool allows inserting a fracture in a pre-existing mesh, with a local modification of the FE model. Input parameters define the geometry and the discretization of the flaw.

Table 2. Main FE model parameters

Parameter	Value
D [mm]	20
D_0 [mm]	16
L [mm]	80
F [kN]	30

As before stated the idea that comes over the paper is the union of mesh morphing and fracture mechanics. Before getting to the point of growth simulation, an important check is the assessment of the crack results obtained from a mesh-morphed model.

3. Results assessment

A three-dimensional FE model was adopted to determine the SIFs values along the crack front. Despite the symmetry of the problem, the whole bar is represented, in such a way the operations of insertion and morph of the crack are accomplished with ease, thanks to the presence of buffer elements all around the affected zone. The mesh is composed by 10-node iso-parametric tetrahedrons. A preliminary check of the model without the flaw is conducted in order to retrieve the stress concentration factor K_t in the reduced section. A convergence test is carried on increasing the number of elements to determine its asymptotic value. The match with the theoretical reference (Pilkey (2008)) occurs for a mesh of 40k elements ($K_{t,FEM}$ =2.214; $K_{t,theory} = 2.2$). However, acceptable correspondences take place also for coarser meshes. A mesh of 29k elements is chosen to be a satisfactory compromise between precision and numerical effort and will be used for fracture mechanics analyses.

As stated before, a baseline crack is inserted in the model by means of the automatic FT. It has the form of an elliptical-arc and is assumed to exist at the notch root (Fig. 1a). Quarter-point wedge elements are used around the

crack front in order to model the stress field singularity. The baseline semi-elliptical crack, used for subsequent morphing actions, was set according to the following parameters: $a = 1.6\,mm$, $\alpha = 1$, $LCR = 0.3\,mm$.

The dimensionless quantities described in the nomenclature are introduced in order to generalize the investigation. Under a tensile load of 30kN a static analysis is run, pointwise values of the SIFs are the desired output. In the present case, the SIFs correspond to K_I in Anderson (2017): mode I of loading. A dimensionless curvilinear abscissa and dimensionless SIF, normalised with respect to h (Fig. 1 a) and reference stress σ_F respectively, are defined as follow:

$$\zeta^* = \frac{\zeta}{h} \tag{10}$$

$$K_I^* = \frac{K_I}{\sigma_F \sqrt{\pi a}} \tag{11}$$

where

$$\sigma_F = \frac{2F}{\pi D_0^2} \tag{12}$$

The first check entails a comparison of dimensionless SIFs along ζ^* for different values of α. A series of flaw geometries are built by means of the FT and, separately, obtained from the baseline configuration by a morphing action. Homologous SIFs distribution are compared pairwise with a perfect match (Fig. 2 a).

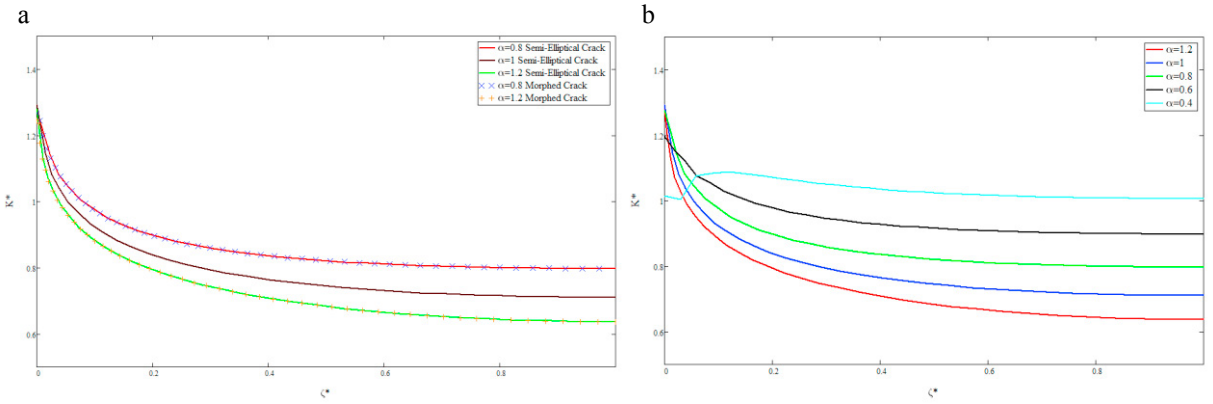

Fig. 2. (a) Comparison of dimensionless SIFs obtained with FT and morphing the baseline configuration; (b) Dimensionless SIFs for Semi-Elliptical cracks obtained with ANSYS FT.

Fig. 2 b shows dimensionless SIFs for different aspect ratios; obtained results are in good agreement with those presented by Carpinteri (2003).

It is useful to provide detailed information on the way the morphing operation was conducted, avoiding an unacceptable degradation of mesh quality. As stated before, wedge elements constitute the appropriate mesh topology to catch the singularity of the stress field. They are arranged in circles, with their tips converging on the line of the crack front. The intersection of the tube of elements along the flaw with the crack plane provides three curves: the central is the trace of the crack front, a tube radius shifts the inner and the outer offset lines from the centre (Fig. 3 a).

a b

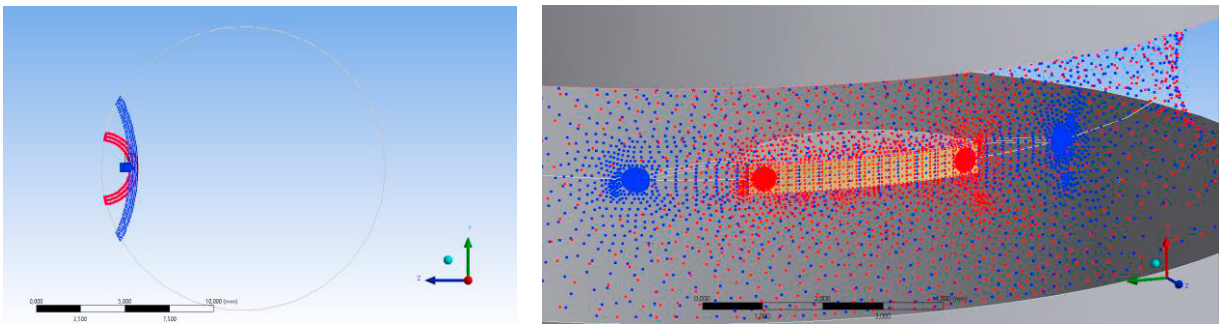

Fig. 3. (a) Auxiliary circle geometries used as support for morphing actions; (b) Nodes preview of mesh morphing.

The displacement field that turns the baseline configuration into a morphed one is assigned relying on these curves. Three new lines on the crack plane identify a new configuration of the flaw. The RBF field is the one that moves each baseline curve onto its new position. A spherical encapsulation of nodes with assigned null motion confines the moulding of the mesh within the desired zone (Fig. 3). It's worth to comment how the RBF set-up is built adopting an auxiliary geometry whilst the morphing action is applied to the nodes of the solid mesh herein managed as a dead mesh without an underlying geometry. We tested this approach because is representative of an industrial scenario where a legacy model representing the cracked component has to be updated onto the new shape resulting from NDT.

4. Parametric analysis

A parametric study starting from a baseline configuration was performed in order to assess the developed approach. Crack shape was modified varying its aspect ratio and its dimensions as reported in Table 3. Prefixed aim is to push the morphing action to the limit, which depends on mesh quality after morphing.

Table 3. Crack shape dimensions for parametric analysis

a [mm]	b [mm]	α []	SIF_{MAX} $[MPa \cdot \sqrt{mm}]$	SIF_{min} $[MPa \cdot \sqrt{mm}]$
1.30	1.30	1.00	400.24	227.95
1.30	1.95	0.66	340.16	262.24
1.30	3.90	0.33	340.93	203.33
1.30	13.00	0.10	356.86	144.48
1.40	1.40	1.00	396.69	237.33
1.40	2.10	0.66	348.92	271.29
1.40	4.20	0.33	350.55	211.02
1.40	14.00	0.10	365.17	156.13
1.60	1.60	1.00	433.75	238.47
1.60	2.40	0.66	368.85	275.16
1.60	4.81	0.33	368.49	238.08
1.60	16.00	0.10	381.13	178.96
1.70	1.70	1.00	394.92	263.64
1.70	2.55	0.66	375.78	296.97
1.70	5.11	0.33	379.40	235.43
1.70	17.00	0.10	390.08	188.27

1.80	1.80	1.00	452.18	245.86
1.80	2.70	0.66	389.13	284.09
1.80	5.40	0.33	386.92	261.38
1.80	18.00	0.10	398.12	201.58

Table 3 shows that, with a proper strategy, mesh morphing can impose large displacement to the mesh, preserving numerical stability. Retrieved results are in line with the expected trends and all the analyses successfully ended up despite mesh deformation. In Fig. 4 it is possible to notice the baseline configuration and the mesh after the morphing action.

a b

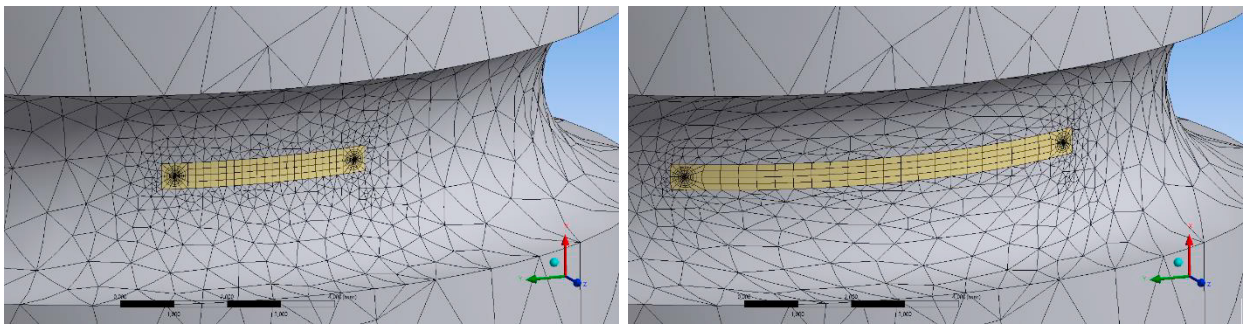

Fig. 4. (a) Baseline crack front in the notched bar; (b) Deformed crack after morphing action.

5. Crack growth simulation

Crack growth follows Paris-Erdogan law:

$$\frac{da}{dN} = C\left(\Delta K_{eff}\right)^m \tag{13}$$

where C and m are material dependent coefficients. In the present case study, the values of such constants were extracted from Afcen (2007). In particular $C = 7.5 \cdot 10^{-10}$ and $m = 4$. A zero-to-maximum load fluctuation (i.e. $\sigma_{min} = 0$) is assumed to compute fatigue parameters for the bar. In this case ΔK_{eff} is equal to the K_I for each node of the crack front.

A direct approach to simulate flaw propagation is to update successively the crack front according to the distribution of the SIFs. Results previously reported showed that the maximum value of K_I is attained at a near-surface point, while its minimum value is encountered at the deepest point. This observation suggests a two-parameter model. A circular arc approximates the crack profile (Fig. 5 a), its centre can move along the symmetry axis of the cross section, in order to represent different aspect ratios. Three points define the circumference providing the arc: two lying on the perimeter of the reduced cross-section (points A and C), a third point on the symmetry axis (point B).

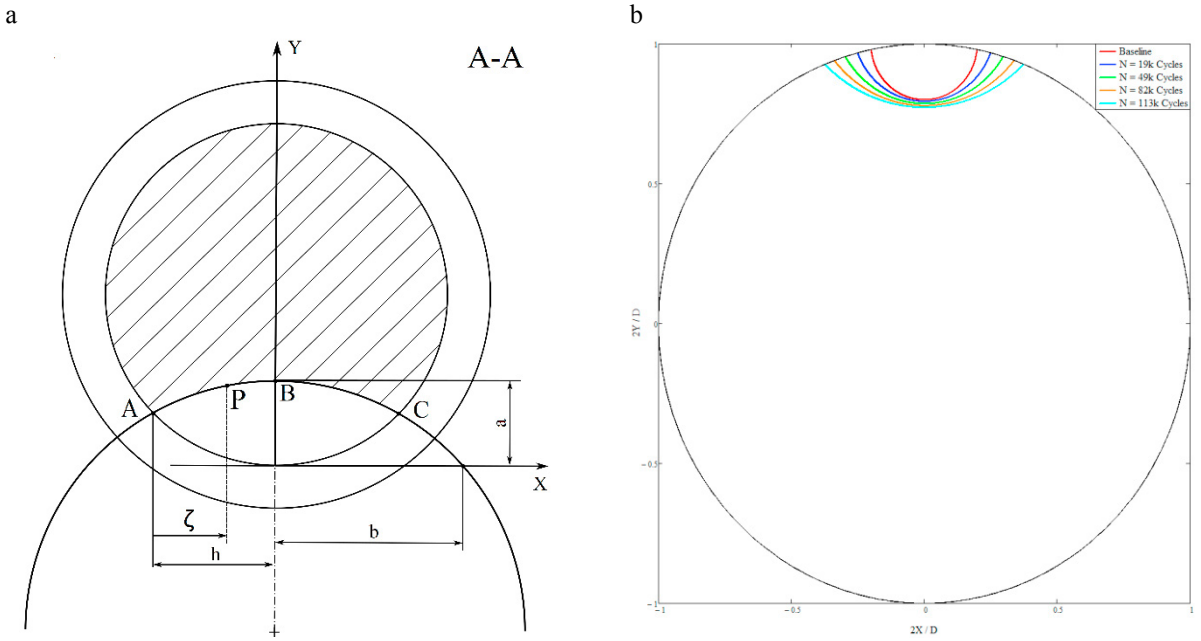

Fig. 5. (a) Circular crack front geometry; (b) Crack front advancement

A FEM analysis supplies the maximum and the minimum values of the SIFs distribution along the crack front. All data necessary to update the flaw profile are thus available. The two outer points of the arc move a given distance δ forward, along the perimeter of the notched section. The advancement of the symmetry point is

$$\Delta a = \delta \left(\frac{K_{\min}}{K_{\max}} \right)^m \tag{14}$$

The corresponding increment of the number of fatigue cycles is

$$\Delta N = \frac{\delta}{C\left(K_{\max}\right)^m} \tag{15}$$

The procedure recurs until a desired N is reached. Fig. 5 b shows the crack advancement obtained with this method. Starting a circular 1.6x1.6 mm configuration the crack front moves into the notched section and after 113k cycles assumes 1.82x3.87 mm dimensions. All the steps between baseline and ending crack shapes are collected in Table 4.

Table 4. Crack front dimensions evolution and related number of cycles.

a [mm]	b [mm]	α []	N_{cyc} [kCycles]	SIF_{MAX} $[MPa \cdot \sqrt{mm}]$	SIF_{min} $[MPa \cdot \sqrt{mm}]$
1.60	1.60	1.00	0	433.75	238.47
1.65	2.15	0.76	18.83	385.89	265.31
1.71	2.56	0.63	48.90	377.55	288.93
1.77	3.27	0.54	81.71	381.82	310.61
1.82	3.48	0.47	113.08		

From Table 4. Crack front dimensions evolution and related number of cycles.it is possible to notice how the crack aspect ratio decreases with the flaw growth.

6. Conclusions

In the present work an assessment of mesh morphing for fracture mechanics is presented. Chosen strategy of morphing is the one adopted by the tool RBFMorph™, relying on RBF. ANSYS® Workbench™ is the framework of investigation. A baseline cracked mesh is morphed to supply a multiplicity of different crack geometries. The same geometries are obtained from scratch, using the Fracture Tool embedded in the ANSYS software. A preliminary comparison showed that fracture analyses conducted on morphed meshes are as reliable as conventional ones, which are performed on mesh obtained from the scratch. Next the limits of applicability of the proposed methodology were investigated by performing a parametric analysis in which different crack shapes were obtained by varying both the crack dimensions and aspect ratios. The methodology proved to be suitable to be used in fracture analyses since the meshes resulted by the application of mesh morphing on the baseline configuration were successfully analysed by the FEM solver, despite the element distortion introduced by the morphing action. Finally the proposed approach was applied to the study of crack growth. A two-parameter geometric description of the crack front shape was adopted allowing the definition of the shape through three points: two on the component surface and one in the deepest point of the crack, assumed to be on the symmetry axis of the planar crack. The displacements of the three points were determined by the use of the Paris-Erdogan law with the maximum and minimum values of the SIFs obtained through FEM analyses: these values were located in the near surface area of the crack and at the deepest point respectively.

The activities presented in the work allow to state that, in the field of fracture mechanics, mesh morphing can give a substantial contribution. Brought advantages mostly regard the reduction of modelling time and the possibility to automate the calculations. Both these aspects play an important role in the simulation of crack growth.

References

Carpinteri, A., Brighenti, R., Spagnoli, A., & Vantadori, S., 2003. Fatigue Growth of Surface Cracks in Notched Round Bars, Proceedings of Fatigue Crack Path. Parma, Italy.

Lin, X. B., & Smith, R. A., 1998. Fatigue growth simulation for cracks in notched and unnotched round bars, International Journal of Mechanical Sciences, 40(5), 405-419.

Murakami, Y., 1986. Stress intensity factors handbook. Soc. Mater. Sci., Japan.

Guo, W., Shen, H., & Li, H., 2003. Stress intensity factors for elliptical surface cracks in round bars with different stress concentration coefficient, International journal of fatigue, 25(8), 733-741.

Paris, P. C., & Erdogan, F., 1963. A critical analysis of crack propagation laws. ASME.

Biancolini, M. E., & Brutti, C., 2002. A numerical technique to study arbitrary shaped cracks growing in notched elements. International Journal of Computer Applications in Technology, 15(4-5), 176-185.

Biancolini, M. E., 2011. Mesh Morphing and Smoothing by Means of Radial Basis Functions (RBF): A Practical Example Using. Handbook of Research on Computational Science and Engineering: Theory and Practice: Theory and Practice, 2, 347.

de Boer, A., Van der Schoot, M. S., & Bijl, H., 2007. Mesh deformation based on radial basis function interpolation. Computers & structures, 85(11), 784-795.

Staten, M. L., Owen, S. J., Shontz, S. M., Salinger, A. G., & Coffey, T. S., 2011. A comparison of mesh morphing methods for 3D shape optimization. In Proceedings of the 20th international meshing roundtable (pp. 293-311). Springer, Berlin, Heidelberg.

Biancolini, M. E., & Cella, U., 2010. An advanced RBF Morph application: Coupled CFD-CSM aeroelastic analysis of a full aircraft model and comparison to experimental data. In Proceedings of the 8th MIRA International Vehicle Aerodynamics Conference (pp. 13-14).

Biancolini, M. E., & Groth, C., 2014. An efficient approach to simulating ice accretion on 2D and 3D airfoils. Advanced Aero Concepts, Design and Operations.

Cella, U., Groth, C., & Biancolini, M. E., 2017. Geometric Parameterization Strategies for shape Optimization Using RBF Mesh Morphing. In Advances on Mechanics, Design Engineering and Manufacturing (pp. 537-545). Springer International Publishing.

Galland, F., Gravouil, A., Malvesin, E., & Rochette, M., 2011. A global model reduction approach for 3D fatigue crack growth with confined plasticity. Computer Methods in Applied Mechanics and Engineering, 200(5), 699-716.

Davis P. J., 1963. Interpolation and approximation, Blaisdell, London.

Anderson, T. L., 2017. Fracture mechanics: fundamentals and applications. CRC press.

Pilkey, W. D., & Pilkey, D. F., 2008. Peterson's stress concentration factors. John Wiley & Sons.

Afcen, R. M., 2007. Design and Construction Rules For Mechanical Components of Nuclear Installations. Section 1 – Subsection Z, Appendix A16: Guide for Leak Before Break Analysis and Defect Assessment.